Homogeneous superconductivity at the LaAlO3/SrTiO3 interface probed by nanoscale transport

Homogeneous superconductivity at the $LaAlO_3/SrTiO_3$ interface probed by nanoscale transport

A. Kalaboukhov,* P. P. Aurino, L. Galletti, T. Bauch, F. Lombardi, D. Winkler, and T. Claeson
Department of Microtechnology and Nanoscience (MC2), Chalmers University of Technology, 412 96 Göteborg, Sweden

D. Golubev
Low Temperature Laboratory, Department of Applied Physics, Aalto University, FI-00076 Aalto, Finland
(Received 24 August 2017; revised manuscript received 6 November 2017; published 29 November 2017)

An interface between $LaAlO_3$ and $SrTiO_3$ (LAO/STO) may host two-dimensional superconductivity, strong spin-orbit coupling, and magnetic ordering. There are indications that the interfacial superconducting layer is nonhomogeneous at the nanoscale. The presence of inhomogeneities may have strong implications on the superconducting transport properties and lead to formation of weak links between superconducting regions. In this paper, we report on the temperature and magnetic field dependence of superconducting transport in single nanowires and nanorings fabricated in a LAO/STO interface. The analysis of data proves that our nanostructures behave like uniform superconducting filaments carrying a critical current close to the theoretical Ginzburg-Landau depairing limit. Furthermore, we unexpectedly find an enhancement of the critical current of LAO/STO nanowires and nanorings at low temperature when a magnetic field is applied. Our results point towards the coexistence of a homogeneous interfacial superconductivity and spatially separated magnetism at the LAO/STO interface.

DOI: 10.1103/PhysRevB.96.184525

I. INTRODUCTION

Advances in oxide thin-film growth have provided routes to structures and phases that are inaccessible by traditional chemical means, and have allowed the properties of existing materials to be modified on the atomic scale [1,2]. The discovery of a two-dimensional electron system (2DES) at the interface between two wide band-gap insulators, $LaAlO_3$ (LAO) and $SrTiO_3$ (STO), that exhibits superconductivity, coexisting with intrinsic ferromagnetism and large gate-tunable spin-orbit coupling (SOC), has stimulated great interest and many experimental and theoretical studies of this system [3,4].

Superconductivity in the LAO/STO interface has many similarities with bulk STO doped with Nb or by oxygen vacancies, having a characteristic transition temperature of $T_C \approx 0.3K$ [5,6]. A two-dimensional character was proven by observation of a Berezinskii-Kosterlitz-Thouless transition [7]. From the temperature dependence of the perpendicular critical field, the Ginzburg-Landau superconducting coherence length was estimated to be $\xi_{GL}(0) \approx 30 - 100$ nm, being higher for the higher carrier concentration [8,9]. The thickness of the superconducting layer is also doping-dependent and was estimated from the anisotropy of parallel and perpendicular magnetic fields to be about 10 nm for optimal doping conditions. However, the thickness may extend up to 100 nm in the overdoped regime [4]. Recent theoretical investigations predicted the possibility of multiband superconductivity driven by the two-dimensional character in the LAO/STO interface [10]. There are also experimental indications of superconducting ordering above the bulk STO critical temperature that may be explained by a two-gap scenario [11,12].

Coexistence of ferromagnetic ordering and superconductivity is one of the most intriguing observations for the LAO/STO interface [13,14]. Moreover, strong Rashba-type SOC was found at the LAO/STO interface [9,15]. A coexistence of superconductivity and ferromagnetism with strong SOC can lead to interesting phenomena, such as chiral p-wave superconductivity [16]. According to theoretical predictions, topological superconducting states may also be found in one dimensional structures of the LAO/STO system [17]. There is no well-established microscopic model that explains how ferromagnetic and superconducting ordering coexist in the LAO/STO. It is possible that superconductivity and ferromagnetism originate from different electronic bands, uniformly distributed in the interface plane. To explain broad superconducting transitions, a nonhomogeneous superconducting state was proposed, where superconducting islands with randomly distributed critical temperatures are embedded in a matrix of weakly localized electrons [18]. The nonhomogeneous distribution can either be driven by defects or by intrinsic electron confinement [19]. It is therefore possible that the superconducting layer consists of superconducting puddles weakly coupled through nonsuperconducting, possibly magnetic, barriers [19,20]. The weak coupling may result in a characteristic Josephson behavior provided that the weak link size is comparable with the superconducting coherence length. If present, such intrinsic Josephson junctions may be an important tool to investigate the paring mechanism in the interfacial superconductor in phase-sensitive experiments. Several works reported superconducting properties in mesoscopic structures of the LAO/STO interface indicating the importance of nonhomogeneous carrier doping [20–22]. However, so far there has been no experimental evidence of any Josephson effect in the LAO/STO interface. Indications of possible 0-π couplings in short point contacts and nanowires in the LAO/STO were recently reported based on observation of minimum critical current at zero magnetic field [22,23].

The goal of this paper was to investigate superconducting transport properties of nanostructures fabricated in the LAO/STO interfacial superconductor. The structures were fabricated using our recently developed technique based on low energy Ar ion implantation [24,25]. An overlay of 1 u.c. $SrCuO_2$ (SCO) was deposited upon 6 u.c. LAO to increase

*alexei.kalaboukhov@mc2.chalmers.se

the electron mobility [25,26] and was followed by a 2 u.c. capping layer of STO. The fabricated nanowires and nanorings have linewidth ranging from 100 to 300 nm, where just few, ideally one, weak link between two superconducting puddles can be formed. Despite expectations, the results show that our nanostructures behave as uniform superconducting filaments without interpuddle weak links. This is supported by very high critical current density approaching the theoretical Ginzburg-Landau depairing limit, and by temperature dependence of switching and retrapping currents. Moreover, we observed an enhancement of the critical current by a small applied magnetic field at low temperatures that can be attributed to the suppression of spin-flip exchange scattering on magnetic impurities.

II. METHODS

Thin films of LAO, SCO, and STO were grown on 5×5 mm^2 large TiO_2-terminated single crystal STO substrates by pulsed lased deposition (PLD). The laser energy density was 1.5 J/cm^2 and the laser spot area on the target was 2 mm^2. The sample was heated to 850 °C and 6 u.c. of LAO were deposited in an oxygen atmosphere of 10^{-4} mbar. The temperature was subsequently decreased to 650 °C and 1 u.c. of SCO was deposited at an oxygen pressure of 6×10^{-2} mbar to improve the 2DES properties. Finally, at the same pressure and temperature, 2 u.c. of STO were deposited as a protecting layer. Samples were not postannealed in oxygen atmosphere after the deposition, but slowly cooled down to room temperature under deposition pressure. The process was monitored using *in situ* reflection high-energy electron diffraction. Intensity oscillations confirmed a layer-by-layer growth. All the samples were inspected by an atomic force microscope (AFM, Bruker Dimension ICON, tapping mode height image) to confirm the smoothness of the surfaces and the presence of 1 u.c. high step terraces.

Nanowires and nanorings in the 2DES were patterned using a low-energy ion beam irradiation technique [24,26]. A resist mask was patterned by e-beam lithography (JEOL JBX-9300FS) in negative resist MicroResist maN2401. The sample was then plasma irradiated by an Ar ion beam in an Oxford IonFab 300 Plus system using an inductively coupled plasma Ar+ source and 3-cm beam aperture. The irradiation time was 1 minutes, with beam energy of 150 eV and a current density of 0.03 mA/cm^2. Low energy and low dose result in a negligible physical etching of the film (maximum 3–4 u.c.) such that the critical thickness of LAO is never reached [24,26]. Furthermore, oxygen vacancies in the STO substrate are not formed by the irradiation.

The nanowires have widths of 200 and 100 nm and fixed width to length ratio of 1:5. Nanorings have linewidths of 300, 200, and 100 nm with a fixed aspect ratio between linewidth and internal diameter of 1:4. The geometry of the nanostructures is shown schematically in Figs. 1(a) and 1(b) and has also been discussed in Ref. [26]. We have earlier performed high-resolution Intermodulation Electrostatic Force Microscopy (ImEFM) imaging of our nanostructures that showed excellent correspondence between expected dimension and electrical contrast, proving confinement of electrical conductivity [25]. Images of thin LAO become more homogeneous when an

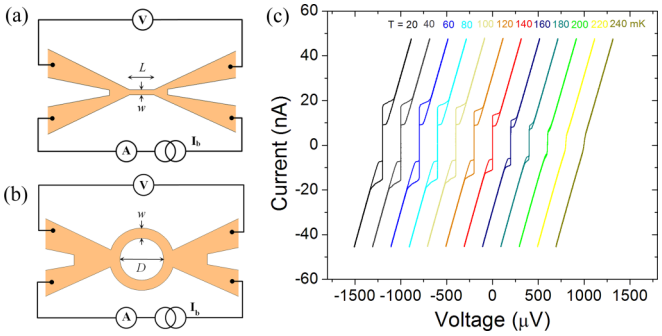

FIG. 1. A sketch of the measured nanowire (a) and nanoring (b) structures. The length of all nanowires, L, is five times larger than their linewidth, w. The inner diameter of all nanorings, D, is four times larger their linewidth, w. (c) A set of current-voltage characteristics (IVC) of a nanoring with linewidth of 100 nm and inner diameter of 400 nm measured in the temperature range of $20 - 240$ mK. Each IVC is a result of 50 averages. The voltage scale was shifted for each IVC by a fixed value to improve the visibility. All IVCs were measured using a current sweep rate of 7 Hz.

SCO cap is used. Critical temperature of nano-structures was obtained from extrapolation of critical current measurements as a function of temperature and estimated to be between 200 and 280 mK for different nanostructures [25].

Electrical connections were provided by DC magnetron sputtering of titanium/gold contact pads with a standard liftoff process. Measurements were performed at cryogenic temperatures down to 20 mK, using a cryogen-free dilution refrigerator (Oxford Triton). The sample was mounted in a metallic Cu box to provide electromagnetic shielding from the environmental noise. A combination of mu-metal shields and a superconducting lead shield granted a protection from the background DC magnetic field component, with a residual field of less than 100 nT. To suppress the effect of noise, twisted pairs of superconducting NbTi/Cu lines were used, in combination with two stages of cryogenic filters. Specifically, a stage of Cu powder filters was installed at the cold stage of the refrigerator, together with low-pass RC filters with a cutoff frequency of 0.2 MHz at the 4 K stage and conventional EMI filters at room temperature. The sample box was equipped with a Helmholtz NbTi/Cu superconducting coil, capable of a maximum magnetic field of 25 mT orthogonal to the sample plane. Room temperature low noise filter amplifiers were used both for conventional pseudo-four-probe measurements of the IV characteristics and the switching currents distribution (SCD).

Conventional time of flight electronics were used for the measurements of the SCD [27]. The bias current was ramped at a rate of 60 μA/s leading to a decay of the junction from the dissipationless to the resistive state [28,29]. After the escape, the bias current is ramped down to zero in 20 ms to cool down the device from the heat locally created in the resistive state.

III. RESULTS

A. Current-voltage characteristics

The evolution of current-voltage characteristics (IVCs) as a function of temperature is presented in Fig. 1(c) for a nanoring with linewidth of 100 nm. All IVCs are characterized by a

TABLE I. A summary of main superconducting parameters of different nanostructures measured at 20 mK: nanowires with linewidth of 100 and 200 nm, and nanorings with linewidth of 100, 200, and 300 nm. The width corresponds to real values measured using atomic force microscopy.

Structure	Width, nm	I_C, nA	J_C, kA/cm^2	R_N, kΩ	$I_C R_N$, μV	I_r/I_C
W100	70	18	2.6	7.0	122	0.45
W200	160	30	2.0	4.6	138	0.33
R100	100	34	1.7	9.2	312	0.25
R200	200	210	5.2	5.2	1100	0.11
R300	300	235	3.9	7.3	1700	0.07

sharp switching from zero to finite voltage states at a critical current, I_C. Above the I_C, all IVCs have linear behavior even at very high bias currents. IVCs show hysteretic behavior at all temperatures with a characteristic retrapping current, I_r, at which switching from finite to zero voltage states occurs. The normal resistance, R_N, of all structures is independent of temperature. No excess current is exhibited in any of the IVCs, i.e., a linear extrapolation of the current above the critical value intersects the origin. The values of I_C, I_r, and R_N for all measured nanostructures are listed in Table I.

The critical current density of our nanostructures can be calculated, assuming a thickness of the superconducting layer of 10 nm [8,9] as $J_C \approx 1{-}5 \times 10^3 A/cm^2$, see Table I. It should be compared with the maximum depairing critical current density in the Ginzburg-Landau theory: $J_{\mathrm{GL}} = \Phi_0/(3\sqrt{3}\pi\mu_0\lambda_L^2\xi)$. Here, $\lambda_L = \sqrt{m^*/\mu_0 n_S e^2}$ is the London penetration depth, $m^* \approx 1.5 m_e$ [30] is the effective electron mass, and n_S is the bulk density of superfluid. Scanning SQUID experiments indicated that sheet superfluid density in the LAO/STO interface is 10 times smaller than the carrier concentration in the normal state, typically about 2×10^{13} cm^{-2} [31]. Assuming this, the estimation of the Ginzburg-Landau critical current density using superconducting layer thickness $t \approx 10$ nm and coherence length $\xi_0 \approx 50$ nm yields $J_{\mathrm{GL}} \approx 5 \times 10^3$ A/cm^2, i.e., the same order of magnitude as the experimental values of J_C. Such very high critical current density is not consistent with a presence of weak links with low transparency. Superconductor-normal metal-superconductor (SNS) weak links with high transparency may have critical current density comparable with the deparing limit, but they are also characterized by a very high excess current of the same order of magnitude as the critical current, which is not observed in our IVCs [32,33]. More information about the transport mechanism can be obtained from analysis of the $I_C R_N$ product. The $I_C R_N$ product depends mainly on the barrier transparency of a weak link. In a serial connection of several weak links, the normal resistance R_N and, correspondingly, the $I_C R_N$ product, increases proportionally with the number of junctions. The $I_C R_N$ product of our nanostructures increases with increasing width and length of the structures. However, the R_N is almost constant and corresponds to the normal resistance defined by the sheet resistance of the nanowire in its normal state (all devices were designed to have approximately the same number of squares). Therefore, the behavior of the $I_C R_N$ product in our nanostructures is also not consistent with the presence of weak links.

B. Temperature dependence of critical current

Further information about the nature of our superconducting nanostructures may be obtained from the temperature dependence of the critical current. Figure 2(a) shows critical current of three devices as a function of temperature normalized to the critical current at 20 mK. In the figure, experimental data are plotted along with the main conventional models to describe $J_C(T)$, specifically the Bardeen dependence for depairing critical current density in a uniform superconducting filament [34] $J_C(T) = J_C(0)(1-(T/T_C)^2)^{3/2}(1+(T/T_C)^2)^{1/2}$ [solid line in Fig. 2(a)], the Ambegaokar-Baratoff dependence for superconductor-insulator-superconductor (SIS) weak links [35,36] $J_C(T) = \pi/2e\rho_n^{-1}\Delta(T)tanh[\Delta(T)/2k_BT]$ [upper dotted line in Fig. 2(a)], the SNS junction with high transparency [37] $J_C(T) = J_C(0)(1-T/T_C)$ [dotted line in Fig. 2(a)], and the SNS junction in the dirty limit, assuming the length of the normal barrier of the same order as the coherence length $J_C(T) = J_C(0)(1-T/T_C)\exp(-0.57L_N/\xi(0)(T/T_C)^{1/2})$ [dashed line in Fig. 2(a)] [38]. As the figure shows, our data are close to temperature dependency of depairing critical current and not efficiently reproduced by models for SNS weak links, especially with high transparency.

C. Analysis of hysteresis

All measured LAO/STO structures show pronounced hysteresis, which is determined by retrapping current I_r. The experimental temperature dependence of the I_r for one of our structures is shown in Fig. 2(b). The $I_r(T)$ for all nanostructures follows the scaling law $I_r(T) \sim \sqrt{(1-(T/T_C)^5}$ [black solid line in the Fig. 2(b)], which is expected in case of Joule heating and dissipation through electron-phonon cooling [39]. This dependence is incompatible with the hypothesis of a conventional resistively and capacitively shunted Josephson junction (RCSJ) model $I_r(T) \sim \sqrt{I_C}$ [40] or with the dynamics of a hot spot formation in SNS junction with scaling behavior of $I_r(T) \sim (T - T_C)^{1/2}$ [41]. Figure 2(b) shows our data along with the best fit, assuming an RCSJ and a hot spot model. It is clear that we can rule out both mechanisms as the origin of the hysteresis in the IVC. The dissipation mechanism can then be described as follows. When the critical current is reached at some spot of the structure, the heat propagates instantaneously along the nanowire, resulting in strong electron overheating to a temperature well above the T_C. The temperature in the equilibrium state is defined by a balance between heating by the bias current and power dissipation from hot electrons to the substrate phonons (neglecting interface Kapitza resistance). In a standard theory of hot electron effect in metal, the power flow is given by $P_{e-\mathrm{ph}} = \Sigma V(T_e^5 - T_{\mathrm{ph}}^5)$, where V is the volume of the metal, Σ is a material constant, T_e is the electron temperature, and T_{ph} is the phonon temperature, which is equal to the bath temperature [39]. The switching to the superconducting state at the bath temperature $T < T_C$ will happen when the electron temperature T_e becomes equal to the critical temperature, T_C. This will be achieved when

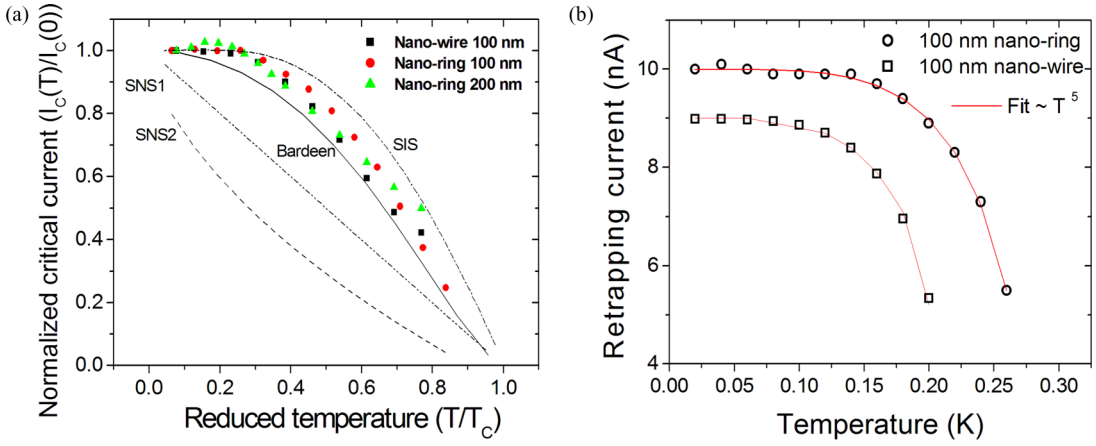

FIG. 2. (a) Normalized critical current $I_C/I_C(20mK)$ as a function of reduced temperature T/T_C for a nanowire with 100-nm width, and two nanorings with 100- and 200-nm linewidths. The solid line corresponds to a fit obtained for a 100-nm nanowire using a model by Bardeen [34]. Upper dash-dotted line corresponds to the Ambegaokar-Baratoff model of SIS junction [35,36]. Bottom dotted and dashed lines correspond to theoretical results for an SNS junction with high transparency [37] and an SNS junction in the dirty limit assuming the length of the normal barrier of the same order as the coherence length [38] (b) Temperature dependence of retrapping current I_r for a nanoring with 100-nm linewidth. Solid line indicates best fitting to the temperature dependence $I_r \sim \sqrt{T_C^5 - T^5}$, indicative of electron-phonon transport of heat.

$I_r(T)^2R = \Sigma V(T_c^5 - T^5)$, or when retrapping current is equal to $I_r(T) = \sqrt{\Sigma V(T_c^5 - T^5)/R}$. From the fitting of data in Fig. 2(b), we obtain $\Sigma V \approx 20nW\mu m^{-3}K^{-5}$ and calculate equilibrium electron temperature for the maximum applied bias current of 1 μA, $T_e = (I^2R/\Sigma V)^5 \approx 2$ K. Assuming that the normal resistance R_N of the nanowire is mainly defined by the local electron temperature, it should follow the $R(T)$ dependence of the nanowire [42]. The resistance of the sample is almost constant at temperatures below 10 K and corresponds to the normal resistance of the nanostructures [25]. This also explains why the normal resistance of nanostructures is constant within the applied current bias and does not depend on temperature. Thus, we conclude that the hysteresis in our nanowires is determined by a Joule heating process and not by phase dynamics in a tilted Josephson washboard potential.

D. Switching current distribution

The switching from superconducting to normal states is a stochastic process, i.e., each time the bias current is swept from zero, the switching occurs at a slightly different bias current. To better understand the switching dynamics, we performed measurements of switching current distribution (SCD) as a function of temperature and magnetic field. Figure 3 shows a set of SCD histograms for the 200-nm ring as a function of temperature. The width of the switching distribution is significantly higher at low temperatures, indicating that the stochastic nature of the switching significantly increases when temperature decreases. This is quantitatively illustrated in the inset in Fig. 3, showing that the standard deviation σ increases for all structures with decreasing temperature. Also, the skewness of the SCD keeps a negative value, which indicates strongly asymmetric histograms, in the whole temperature range. This behavior is characteristic of multiple thermally activated phase slips (TAPS) in narrow superconducting filaments [43,44]. The phase slip dynamics depend on the balance between heat produced in a single TAPS event and power dissipation. At high temperatures, multiple TAPS are often required to trigger switching. As temperature decreases, the electron-phonon thermal conductivity rapidly decreases and TAPS are more effective to activate switching. This increases internal stochasticity and explains broadening of σ with lowering temperature [44]. In a multiple TAPS scenario, the SCDs are asymmetric due to premature switching below the I_C [45]. This behavior is opposite to classical weak-link behavior where the standard deviation usually

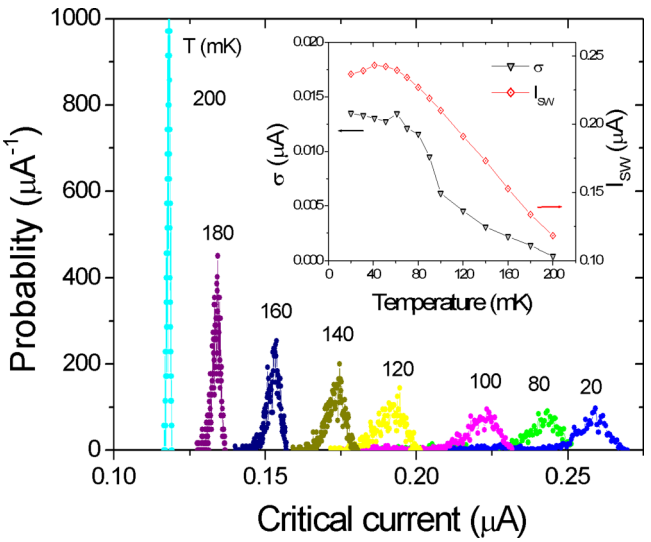

FIG. 3. Switching current distributions of the nanoring with 200-nm linewidth measured at different temperatures below the T_C. The inset shows temperature dependencies of the switching current I_{SW} (triangles) and standard deviation σ (open diamonds) of the SCD for the same nanoring. Note that σ monotonically increases with decreasing temperature, while switching current decreases at the lowest temperatures.

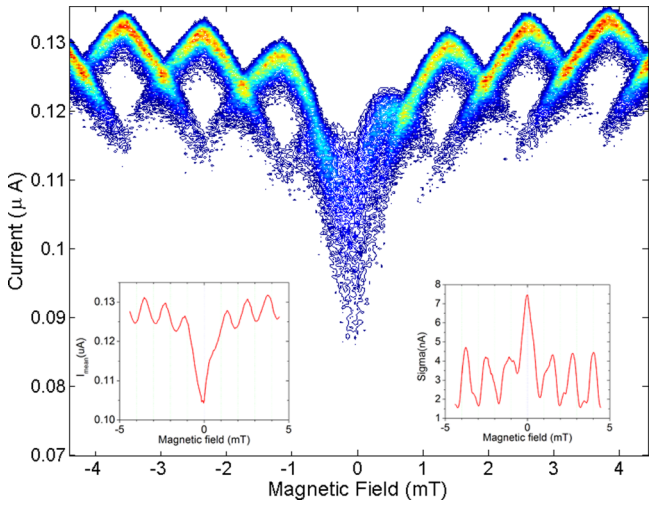

FIG. 4. Switching current distribution for a ring with 300-nm linewidth, as a function of magnetic field, measured at 20 mK. The inset on the left shows the mean value of the switching current, while the right inset shows its width σ, both as a function of the magnetic field. Note that the appearance of two current distributions, shifted by a flux quantum (that corresponds to 1.3 mT), indicates a bistable nature.

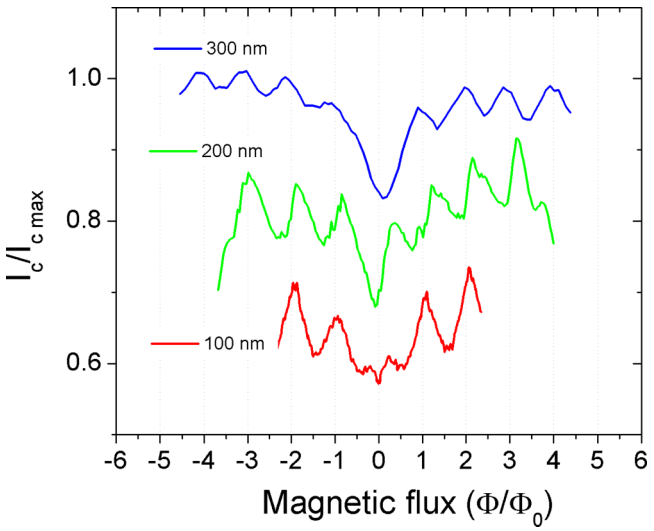

FIG. 5. Normalized critical current as a function of magnetic flux normalized to the single flux quantum for nanorings with linewidths of 100, 200, and 300 nm and inner diameters of 400, 800, and 1200 nm. All measurements were performed at 20 mK. For clarity, the curves corresponding to 200 nm and 100 nm are intentionally shifted by −0.2 and −0.4, respectively. Magnetic flux in the nanoring was calculated using an effective area defined by inner-ring radius plus half of the linewidth (see main text). Interference between oscillations with flux and a dip in critical current centered around zero field complicates the appearance of the curve at low flux.

decreases in the thermally activated regime and saturates below a cross-over temperature corresponding to the macroscopic quantum tunneling regime [46]. It is possible that the width of transition increases with decreasing temperature due to multiple retrapping (phase diffusion) in moderately damped Josephson junctions [47,48]. A Josephson junction with a moderate quality factor $Q \approx 1$ and low Josephson energy $E_J = \hbar I_C/2e$ may stay in the phase diffusion regime in the full temperature range [49]. However, we note that the phase diffusion causes symmetrization of the SCDs [29]. Thus we conclude that switching from superconducting to normal states in our nanowires is governed by multiple TAPS, rather than by Josephson dynamics.

E. Magnetic field dependence

The SCD as a function of magnetic field for a nanoring with 300-nm linewidth measured at 20 mK is shown in Fig. 4. The switching current shows periodic oscillations as a function of magnetic field. The oscillations have triangular shape and there are regions where the switching current is multivalued. We note that σ also periodically oscillates with magnetic field while the retrapping current is field independent. This is more evidence that the switching dynamics are governed by phase slips events. To understand the origin of the oscillations, we have plotted the critical current of three nanorings as a function of magnetic flux, see Fig. 5. The flux in each nanoring was calculated assuming the effective area $A_{\text{eff}} = \pi(R + w/2)^2$, where R is the inner ring radius and w is the linewidth. The period of oscillations corresponds well to one single flux quantum $\Phi_0 = h/2e$ in all nanorings. The behavior resembles a DC SQUID with two Josephson junctions and its sinusoidal periodic modulation of critical current with a period corresponding to an integer number of single flux quanta [40]. However, the behavior of our nanorings is qualitatively different from classical DC SQUIDs: modulation is not sinusoidal, and the critical current is a multivalued periodic function of the magnetic field. A similar effect was previously reported in micro-SQUIDs with weak links formed by Dayem bridges [50,51], in YBCO nanowire SQUIDs [52], and asymmetric MoGe nanowire SQUIDs [53]. A long nanowire with $L > \xi$ has very high kinetic inductance that results in a large phase gradient and nonsinusoidal current-phase relationship along the nanowire [40]. The periodic critical current modulation appears due to fluxoid quantization [54] and interference between screening current caused by applied magnetic flux and currents in two arms of the superconducting ring.

Another remarkable feature that can be seen in Fig. 4 is the minimum of the critical current at zero magnetic field. The minimum develops at low temperature (below 100 mK) and appears in all nanorings and nanowires. Figure 6 shows magnetic field dependence of the critical current for nanorings and nanowires with linewidths of 100 and 200 nm taken at 20 mK (the data in Fig. 6 are taken in a wider range of magnetic field as compared to Fig. 4). The nanowires do not show periodic oscillations but the minimum of critical current is clearly visible and has a very similar envelope as in the nanorings. Such an effect may be caused by an intrinsic π phase shift due to the presence of a ferromagnetic barrier in the Josephson junction [55]. However, we did not observe the Fraunhofer pattern of the current-field dependence typical for Josephson junctions [40]. Moreover, the critical current may exhibit a minimum at zero magnetic field only in a hybrid Josephson junction containing both 0 and π regions [56]. The practical realization of such a hybrid junction is very complicated due to nonmonotonic dependence of the critical

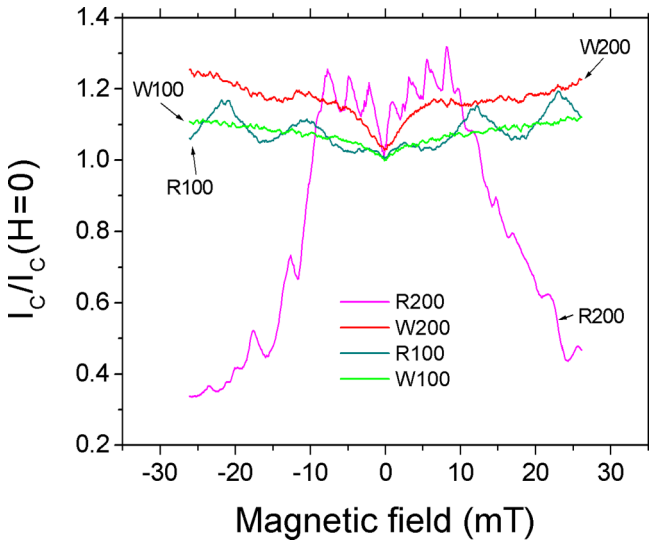

FIG. 6. Comparison of the magnetic field dependence of the critical current for nanowires and nanorings. R100, R200, and W100, W200 indicate nanorings and nanowires with 100- and 200-nm linewidths. Measurements were performed at 20 mK. No critical current oscillations are observed in nanowires. The dip at zero magnetic field is seen in all structures and has similar envelope in nanowires and nanorings.

current on temperature and ferromagnetic barrier thickness [57]. It is therefore implausible that the minimum of critical current in our nanostructures is due to interference effect in the $0-\pi$ Josephson junction. Instead, there should be a common mechanism of critical current suppression that is counteracted by a small magnetic field. First, we can exclude flux trapping effects as no hysteresis in magnetic field is observed, and magnetic field patterns for both positive and negative current biases are fully centrosymmetric.

The fact that the dip in critical current at zero magnetic field is similar in structures with different geometries suggests that it may be of local origin, i.e., associated with magnetic spins rather than interference of supercurrents. The superconductivity is normally suppressed in the presence of uncorrelated and unpolarized magnetic impurities as pairs are broken by spin-flip scattering. However, the critical temperature and critical current is partially restored by a small magnetic field that polarizes spins and suppresses spin-flip exchange scattering [58]. The enhancement of the critical current is more pronounced at low temperature due to stronger polarization of magnetic impurities. A similar behavior was observed in MoGe, Nb [59], and proximity Al-Au [60] superconducting nanowires. In addition, the scale of the magnetic field where the enhancement is observed depends on an interplay between exchange interactions and paramagnetic and orbital effects that also suppress superconductivity [61]. In addition, strong SOC weakens the depairing by orbital effects [62]. A simple estimation of the magnetic field scale is given by $B \approx 0.1 k_B T_C/\mu_B \approx 35mT$ for the $T_C = 0.25K$ [61], which is in a good agreement with our experimental results. These qualitative arguments imply that the observed minimum of critical current at zero magnetic field in our nanostructures may be caused by suppression of spin-flip exchange interactions.

IV. DISCUSSION

Previous calculations have suggested an inhomogeneous state at the interface with loosely connected superconducting puddles to explain broadening of superconducting transition [11]. We find that the superconductivity in our LAO/STO nanostructures is homogeneous, as the critical current is close to the maximum theoretical depairing limit. We also did not observe characteristic Josephson behavior in our nanostructures. The results thus do not support the existence of weakly coupled superconducting puddles. We also unexpectedly find that there is an enhancement of the critical current of LAO/STO nanowires and nanorings at low temperature when a magnetic field is applied. These results may be understood as the superconducting pairs presumably reside in a region in STO below the interface while inhomogeneities may be due to an uneven distribution of Ti magnetic moments at the interface caused, for example, by oxygen vacancies, intermixing, Ti-O octahedra tipping, or strain. The presence of magnetic spins may suppress locally the critical temperature of the superfluid and result in a broad superconducting transition. Well below the critical temperature the superfluid is homogeneous, but the critical current is suppressed by unpolarized magnetic spins. A small magnetic field polarizes the spins that reduces spin-flip exchange scattering, resulting in an enhancement of the critical current, as observed in all our nanostructures.

While we have no direct evidence for the presence of magnetic impurities in our samples, magnetism in the LAO/STO interface has been widely reported [13,14,63]. There is a very large spread of magnetic ordering temperatures, from several hundreds of mK to 300 K. We have carefully investigated magneto-transport properties of our samples down to 2 K and could not see any characteristic features of the magnetic ordering (resistivity upturn due to Kondo effect, hysteresis in longitudinal magneto-resistance, and anomalous Hall effect). This implies that the ordering of magnetic impurities in our samples is at least below 2 K. This is in agreement with recent observation of hysteresis curves in magnetoresistance of LAO/STO nanowires below 1 K that was attributed to the presence of in-plane antiferromagnetic ordering with characteristic energy corresponding to a field of 100 G at 20 mK [64]. This magnetic field scale strikingly coincides with the dip in the critical current in our data, providing additional support for the presence of magnetism in our samples.

We finally note that our results were obtained in optimally doped samples corresponding to the maximum of critical temperature. It is pointed out that the electron gas may become more inhomogeneous at low carrier concentrations [65]. Therefore, it will be interesting to measure superconducting transport in the LAO/STO nanowires as a function of carrier concentration.

V. CONCLUSIONS

Our results shed light on the microscopic nature of two-dimensional superconductivity in the LAO/STO interface. We propose a model where the homogeneous superconducting layer is spatially separated from the magnetic spins. These findings are important for designing superconducting devices based on the LAO/STO interface, in particular for search of theoretically predicted topological superconductivity.

ACKNOWLEDGMENTS

We thank M. Fogelström, T. Löfwander, M. Kupriyanov, and A. Balatsky for useful discussions. This paper was supported by the Swedish Research Council (Vetenskapsrådet) Grant No. 2016-05256 and the Knut and Alice Wallenberg Foundation (Knut och Alice Wallenbergs Stiftelse), and the Swedish Institute Visby program. The support from the Swedish infrastructure for micro- and nanofabrication, Myfab, is appreciated.

[1] J. A. Sulpizio, S. Ilani, P. Irvin, and J. Levy, Annu. Rev. Mater. Res. **44**, 117 (2014).
[2] N. Setter, D. Damjanovic, L. Eng, G. Fox, S. Gevorgian, S. Hong, A. Kingon, H. Kohlstedt, N. Y. Park, G. B. Stephenson, I. Stolitchnov, A. K. Taganstev, D. V. Taylor, T. Yamada, and S. Streiffer, J. Appl. Phys. **100**, 051606 (2006).
[3] A. Ohtomo and H. Hwang, Nature **427**, 423 (2004).
[4] S. Gariglio, M. Gabay, and J.-M. Triscone, APL Mater. **4**, 060701 (2016).
[5] C. S. Koonce, M. L. Cohen, J. F. Schooley, W. R. Hosler, and E. R. Pfeiffer, Phys. Rev. **163**, 380 (1967).
[6] J. F. Schooley, H. P. R. Frederikse, W. R. Hosler, and E. R. Pfeiffer, Phys. Rev. **159**, 301 (1967).
[7] N. Reyren, S. Thiel, A. D. Caviglia, L. Fitting-Kourkoutis, G. Hammer, C. Richter, C. W. Schneider, T. Kopp, A.-S. Rüuetschi, D. Jaccard, M. Gabay, D. A. Muller, J.-M. Triscone, and J. Mannhart, Science **317**, 1196 (2007).
[8] N. Reyren, S. Gariglio, A. D. Caviglia, D. Jaccard, T. Schneider, and J.-M. Triscone, Appl. Phys. Lett. **94**, 112506 (2009).
[9] M. B. Shalom, M. Sachs, D. Rakhmilevitch, A. Palevski, and Y. Dagan, Phys. Rev. Lett. **104**, 126802 (2010).
[10] R. M. Fernandes, J. T. Haraldsen, P. Wölfle, and A. V. Balatsky, Phys. Rev. B **87**, 014510 (2013).
[11] D. Bucheli, S. Caprara, and M. Grilli, Supercond. Sci. Technol. **28**, 045004 (2015).
[12] C. Richter, H. Boschker, W. Dietsche, E. Fillis-Tsirakis, R. Jany, F. Loder, L. F. Kourkoutis, D. A. Muller, J. R. Kirtley, C. W. Schneider, and J. Mannhart, Nature **502**, 528 (2013).
[13] J. A. Bert, B. Kalisky, C. Bell, M. Kim, Y. Hikita, H. Y. Hwang, and K. A. Moler, Nature Phys. **7**, 767 (2011).
[14] D. A. Dikin, M. Mehta, C. W. Bark, C. M. Folkman, C. B. Eom, and V. Chandrasekhar, Phys. Rev. Lett. **107**, 056802 (2011).
[15] A. D. Caviglia, M. Gabay, S. Gariglio, N. Reyren, C. Cancellieri, and J.-M. Triscone, Phys. Rev. Lett. **104**, 126803 (2010).
[16] K. Michaeli, A. C. Potter, and P. A. Lee, Phys. Rev. Lett. **108**, 117003 (2012).
[17] L. Fidkowski, H.-C. Jiang, R. M. Lutchyn, and C. Nayak, Phys. Rev. B **87**, 014436 (2013).
[18] S. Caprara, J. Biscaras, N. Bergeal, D. Bucheli, S. Hurand, C. Feuillet-Palma, A. Rastogi, R. C. Budhani, J. Lesueur, and M. Grilli, Phys. Rev. B **88**, 020504(R) (2013).
[19] N. Scopigno, D. Bucheli, S. Caprara, J. Biscaras, N. Bergeal, J. Lesueur, and M. Grilli, Phys. Rev. Lett. **116**, 026804 (2016).
[20] G. E. D. K. Prawiroatmodjo, F. Trier, D. V. Christensen, Y. Chen, N. Pryds, and T. S. Jespersen, Phys. Rev. B **93**, 184504 (2016).
[21] D. Stornaiuolo, S. Gariglio, N. J. G. Couto, A. Fête, A. D. Caviglia, G. Seyfarth, D. Jaccard, A. F. Morpurgo, and J.-M. Triscone, Appl. Phys. Lett. **101**, 222601 (2012).
[22] V. V. Bal, M. M. Mehta, S. Ryu, H. Lee, C. M. Folkman, C. B. Eom, and V. Chandrasekhar, Appl. Phys. Lett. **106**, 212601 (2014).
[23] D. Stornaiuolo, D. Massarotti, R. Di Capua, P. Lucignano, G. P. Pepe, M. Salluzzo, and F. Tafuri, Phys. Rev. B **95**, 140502(R) (2017).
[24] P. P. Aurino, A. Kalabukhov, N. Tuzla, E. Olsson, T. Claeson, and D. Winkler, Appl. Phys. Lett **102**, 201610 (2013).
[25] P. P. Aurino, A. Kalabukhov, R. Borgani, D. B. Haviland, T. Bauch, F. Lombardi, T. Claeson, and D. Winkler, Phys. Rev. Appl. **6**, 024011 (2016).
[26] P. P. Aurino, A. Kalabukhov, N. Tuzla, E. Olsson, A. Klein, P. Erhart, Y. A. Boikov, I. T. Serenkov, V. I. Sakharov, T. Claeson, and D. Winkler, Phys. Rev. B **92**, 155130 (2015).
[27] T. Bauch, F. Lombardi, F. Tafuri, A. Barone, G. Rotoli, P. Delsing, and T. Claeson, Phys. Rev. Lett. **94**, 087003 (2005).
[28] V. M. Krasnov, T. Golod, T. Bauch, and P. Delsing, Phys. Rev. B **76**, 224517 (2007).
[29] L. Longobardi, D. Massarotti, G. Rotoli, D. Stornaiuolo, G. Papari, A. Kawakami, G. P. Pepe, A. Barone, and F. Tafuri, Phys. Rev. B **84**, 184504 (2011).
[30] A. D. Caviglia, S. Gariglio, C. Cancellieri, B. Sacepe, A. Fete, N. Reyren, M. Gabay, A. F. Morpurgo, and J.-M. Triscone, Phys. Rev. Lett. **105**, 236802 (2010).
[31] J. A. Bert, K. C. Nowack, B. Kalisky, H. Noad, J. R. Kirtley, C. Bell, H. K. Sato, M. Hosoda, Y. Hikita, H. Y. Hwang, and K. A. Moler, Phys. Rev. B **86**, 060503(R) (2012).
[32] G. E. Blonder, M. Tinkham, and T. M. Klapwijk, Phys. Rev. B **25**, 4515 (1982).
[33] A. A. Golubov, V. M. Krasnov, and M. Yu. Kupriyanov, IEEE Trans. Appl. Supercond. **7**, 3204 (1997).
[34] J. Bardeen, Rev. Mod. Phys. **34**, 667 (1962).
[35] V. Ambegaokar and A. Baratoff, Phys. Rev. lett. **10**, 486 (1963).
[36] Y.-d. Song and G. I. Rochlin, Phys. Rev. Lett. **29**, 416 (1972).
[37] K. A. Delin and A. W. Kleinsasser, Supercond. Sci. Tech. **9**, 227 (1996).
[38] V. G. Prokhorov, G. G. Kaminsky, Y. P. Lee, and I. I. Kravchenko, J. Low Temp. Phys. **26**, 881 (2000).
[39] R. L. Kautz and J. M. Martinis, Phys. Rev. B **42**, 9903 (1990).
[40] M. Tinkham, *Introduction to Superconductivity: Second Edition* (McGraw-Hill, Inc., New York, 1996).
[41] W. J. Skocpol, M. R. Beasley, and M. Tinkham, J. Low Temp. Phys **16**, 145 (1974).
[42] M. Tinkham, J. U. Free, C. N. Lau, and N. Markovic, Phys. Rev. B **68**, 134515 (2003).
[43] N. Shah, D. Pekker, and P. M. Goldbart, Phys. Rev. Lett. **101**, 207001 (2008).
[44] M. Sahu, M.-H. Bae, A. Rogachev, D. Pekker, T.-C. Wei, N. Shah, P. M. Goldbart, and A. Bezryadin, Nat. Phys. **5**, 503 (2009).
[45] D. Pekker, N. Shah, M. Sahu, A. Bezryadin, and P. M. Goldbart, Phys. Rev. B **80**, 214525 (2009).
[46] T. A. Fulton and L. N. Dunkleberger, Phys. Rev. B **9**, 4760 (1974).

[47] J. M. Kivioja, T. E. Nieminen, J. Claudon, O. Buisson, F. W. J. Hekking, and J. P. Pekola, Phys. Rev. Lett. **94**, 247002 (2005).
[48] V. M. Krasnov, T. Bauch, S. Intiso, E. Hurfeld, T. Akazaki, H. Takayanagi, and P. Delsing, Phys. Rev. Lett. **95**, 157002 (2005).
[49] L. Longobardi, D. Massarotti, D. Stornaiuolo, L. Galletti, G. Rotoli, F. Lombardi, and F. Tafuri, Phys. Rev. Lett. **109**, 050601 (2012).
[50] M. Faucher, T. Fournier, B. Pannetier, C. Thirion, W. Wernsdorfer, J. C. Villegier, and V. Bouchiat, Physica C **368**, 211 (2002).
[51] A.K. H. Lam, J. R. Clem, and W. Yang, Nanotechnology **22**, 455501 (2011).
[52] R. Arpaia, S. Charpentier, R. Toskovic, T. Bauch, and F. Lombardi, Physica C **506**, 184 (2014).
[53] A. Murphy and A. Bezryadin, Phys. Rev. B **96**, 094507 (2017).
[54] R. D. Perks and W. A. Little, Phys. Rev. **133**, A97 (1964).
[55] A. A. Bannykh, J. Pfeiffer, V. S. Stolyarov, I. E. Batov, V. V. Ryazanov, and M. Weides, Phys. Rev. B **79**, 054501 (2009).
[56] M. Weides, M. Kemmler, H. Kohlstedt, R. Waser, D. Koelle, R. Kleiner, and E. Goldobin, Phys. Rev. Lett. **97**, 247001 (2006).
[57] V. V. Ryazanov, V. A. Oboznov, A. Yu. Rusanov, A. V. Veretennikov, A. A. Golubov, and J. Aarts, Phys. Rev. Lett. **86**, 2427 (2001).
[58] M. Yu. Kharitonov and M. V. Feigelman, JETP Lett. **82**, 421 (2005).
[59] A. Rogachev, T.-C. Wei, D. Pekker, A. T. Bollinger, P. M. Goldbart, and A. Bezryadin, Phys. Rev. Lett. **97**, 137001 (2006).
[60] L. Angers, F. Chiodi, G. Montambaux, M. Ferrier, S. Guéron, H. Bouchiat, and J. C. Cuevas, Phys. Rev. B **77**, 165408 (2008).
[61] T.-C. Wei, D. Pekker, A. Rogachev, A. Bezryadin, and P. M. Goldbart, Europhys. Lett., **75**, 943 (2006).
[62] P. Fulde and K. Maki, Phys. Rev. **141**, 275 (1966).
[63] L. Li, C. Richter, J. Mannhart, and R. Ashoori, Nat. Phys. **7**, 762 (2011).
[64] A. Ron, E. Maniv, D. Graf, J.-H. Park, and Y. Dagan, Phys. Rev. Lett. **113**, 216801 (2014).
[65] G. Singh, A. Jouan, L. Benfatto, F. Couedo, P. Kumar, A. Dogra, R. Budhani, S. Caprara, M. Grilli, E. Lesne, A. Barthelemy, M. Bibes, C. Feuillet-Palma, J. Lesueur, and N. Bergeal, arXiv:1704.03365v1.